Co-Targeting BCL-xL with MCL-1 Induces Lethal Mitochondrial Dysfunction in Diffuse Mesothelioma

Yuan Xu[1], Cristian G. Medina[1], Deborah R. Surman[2], Lacey E. Dobrolecki[3], Monica Vilchis[1], Maheshwari Ramineni[4], Susan G. Hilsenbeck[3], Yanming Li[5,6], Naren Li[1], Siqi Wu[1], Jaylon C. Aggison[1], Xi Chen[7], Yi Zhu[7], Ying H. Shen[5,6], and R. Taylor Ripley[1]

ABSTRACT

Diffuse mesothelioma is a rare but highly aggressive and treatment-resistant neoplasm with low survival rates. Effective therapeutic strategies are limited, and resistance to treatment is a major obstacle. Myeloid cell leukemia (MCL)-1 and B-cell leukemia (BCL)-xL are antiapoptotic B-cell lymphoma 2 (Bcl-2) family proteins that block cell-intrinsic apoptosis through interactions on the mitochondrial outer membrane which contribute to therapeutic resistance. We investigated whether B-cell homology domain3 profiles were consistent between intra-patient fresh tumor sample, patient-derived cells, and patient-derived xenografts (PDX) by B-cell homology domain-3 profiling; we observed striking consistency which enabled cross-model comparisons. Next, we co-targeted BCL-xl and MCL-1 and noted that the combination synergistically reduced cell viability and increased apoptosis. Mechanistically, BCL-xL inhibition affected the cells through both the canonical and the emerging noncanonical apoptotic pathways. BCL-xL induced mitochondrial depolarization which resulted in MCL-1 cellular dependency, rendering cells highly sensitive to MCL-1 inhibition. Next, we co-targeted BCL-xL and MCL-1 *in vivo* which induced synthetic lethality in PDX models within hours, implying that this approach is not a safe strategy for clinical development. However, targeting MCL-1, which exerts its antiapoptotic activity without non-apoptotic on-target effects, decreased the mitochondrial threshold for apoptosis and enhanced chemosensitivity without toxicity in PDX models. Our findings suggest that targeting the mitochondria via MCL-1 enhances the efficacy of chemotherapy but co-targeting two proteins in the Bcl-2 pathways results in synergistic lethality. These results will help define a safe clinical strategy to utilize Bcl-2–targeted therapy to undermine therapeutic resistance in patients with diffuse mesothelioma.

Introduction

Diffuse mesothelioma arises from neoplastic transformation of mesothelial cells lining the pleural cavities and has 5-year overall survival under 10% (1). The chemotherapeutic agents, cisplatin (CDDP) and pemetrexed, were US FDA-approved based on a median overall survival benefit from 9.3 to 12.1 months in 2004 (1). Alternative therapies have minimally affected survival until 2021 with the landmark trial, CHECKMATE 743, of immune checkpoint inhibitors (2). Despite some improvements with systemic chemotherapy or immunotherapy, responses only occur in a subset of patients and resistance is common.

Cell-intrinsic apoptosis, in part, occurs through the mitochondria via the balance of B-cell lymphoma 2 (Bcl-2) family of proteins (3, 4). Targeting antiapoptotic Bcl-2 proteins to undermine apoptotic resistance led to a class of small-molecule inhibitors known as B-cell homology domain-3 (BH3) mimetics (3). BH3 mimetics directly target the pro-survival Bcl-2 proteins to sensitize cells to cell death by mitochondrial outer membrane permeabilization (MOMP; refs. 5, 6). Our previous work showed that diffuse mesothelioma and esophageal adenocarcinoma (EAC) resist apoptosis through the upregulation of myeloid cell leukemia (MCL)-1; moreover, targeting MCL-1 changed the threshold for apoptosis which enhanced sensitivity to chemotherapy (7, 8). The antiapoptotic Bcl-2 proteins have redundant functions; therefore, targeting one protein may upregulate other non-targeted antiapoptotic Bcl-2 proteins to ensure tumor cell survival. Therefore, co-targeting MCL-1 with B-cell leukemia (BCL)-xL is a logical strategy to prevent their redundant functions (9, 10). Several pharmaceutical companies are currently developing BH3 mimetics for clinical trials; the FDA has approved the first BH3 mimetic, venetoclax, an oral Bcl-2 inhibitor to treat chronic lymphocytic leukemia and acute myeloid leukemia (11), but a major obstacle associated with these strategies is on-target, dose-limiting toxicity (12, 13). Therefore, evaluation of mechanisms of co-targeting these proteins is critically important to ensure safe introduction into clinical trials.

BH3 profiling is a live cell functional bioassay that identifies cellular dependence on individual antiapoptotic proteins and predicts cellular response to chemotherapy agent and identifies which Bcl-2 proteins are responsible for resistance to apoptosis (7, 14). The pro- and antiapoptotic Bcl-2 proteins that regulate MOMP interact with one another at the hydrophobic BH3 domains. BH3 profiling measures the relative interactions of these proteins to determine

[1]David J. Sugarbaker Division of Thoracic Surgery, Michael E. DeBakey Department of Surgery and the Dan L Duncan Comprehensive Cancer Center, Baylor College of Medicine, Houston, Texas. [2]Michael E. DeBakey Department of Surgery, Baylor College of Medicine, Houston, Texas. [3]Lester and Sue Smith Breast Center, Baylor College of Medicine, Houston, Texas. [4]Department of Pathology and Immunology, Baylor College of Medicine, Houston, Texas. [5]Division of Cardiothoracic Surgery, Michael E. DeBakey Department of Surgery, Baylor College of Medicine, Houston, Texas. [6]Department of Cardiovascular Surgery, The Texas Heart Institute, Houston, Texas. [7]Department of Pediatrics, Children's Nutrition Research Center, Baylor College of Medicine, Houston, Texas.

Corresponding Author: R. Taylor Ripley, Meyer DeBakey Chair of Investigative Surgery, David J. Sugarbaker Division of Thoracic Surgery, Michael E. DeBakey Department of Surgery, Baylor College of Medicine, 7200 Cambridge Street, Houston, TX 77030. E-mail: R.Taylor.Ripley@bcm.edu

Mol Cancer Ther 2025;24:1640–52

doi: 10.1158/1535-7163.MCT-24-0873

whether a tumor cell is near the threshold to activate apoptosis ("priming"; refs. 14, 15), which predict response to chemotherapy and resistance to targeted therapy in both clinical samples and cell culture (16). We previously performed BH3 profiling directly on fresh patient tumors of EAC and diffuse mesothelioma and identified proteins responsible for resistance (7). Although BH3 profiling is a predictive tool for assessing mitochondrial apoptotic sensitivity, it has not yet undergone sufficient large-scale clinical studies to verify its reliability and predictive power for drug response to determine therapy for patients. Validation of BH3 profiling in patient samples to rapidly assess drug sensitivity is significant to enable clinically feasible time frames as compared with cell culture or mouse models.

In this study, we examined whether co-targeting MCL-1 and BCL-xL is a safe therapeutic strategy. We expect that BH3 profiling in fresh tumor will serve as a live cell, predictive bioassay to identify which patient's tumors will respond to BH3 mimetics. Additionally, we expect to establish a safe strategy to introduce BH3 mimetics into clinical trials. Our findings will provide insights into the mechanisms of synergistic effects of targeting Bcl-2 proteins on canonical and noncanonical apoptotic pathways with the goal of undermining therapeutic resistance.

Materials and Methods

Cell culture and regents

Cell lines H28 and H2452 were purchased from ATCC. All cell lines were authenticated yearly with HLA analysis and tested for *Mycoplasma* contamination every six months. Cells were cultured in RPMI (Thermo Fisher Scientific) supplemented with 10% FCS and 1% penicillin/streptomycin (Gibco). BCL-2 inhibitor, ABT199, was purchased from APExBIO; MCL-1 inhibitor, AZD5991 (17), and BCL-xL inhibitor, A11554639 (18), were purchased from MedChemExpress; and CDDP was purchased from APP Pharmaceuticals. Detail information of all reagents is specified in Supplementary Table S1.

Primary cells

Mesothelioma tumor specimens were obtained from patients at Baylor College of Medicine and Affiliated Hospitals with Institutional Review Board approval (H46562), and written informed consent was obtained from each participant. Patients' information is specified in Supplementary Table S2. Tumor samples were obtained by biopsy or surgical resection and then minced and dissociated using the human tumor dissociation kit (Miltenyi Biotec). Samples were either incubated at 37°C while gently rocking for 1 hour or dissociated using the gentleMACS system following the manufacturer's protocol. After dissociation, the suspension was filtered through a 70-μm cell strainer (BD Falcon) and washed with PBS.

BH3 profiling

Intracellular BH3 profiling has been previously described in detail (14, 19). Single-cell processing of solid tumors was performed by manually cutting into multiple pieces and then digesting by gentleMACS Dissociator (Miltenyi Biotec). After generating single cells, for BH3 profiling, primary cells were first stained with viability dye, LIVE/DEAD Fixable Aqua (Thermo Fisher Scientific), washed, and then incubated with FcR blocking reagent and surface stained with PE anti–human podoplanin (D2-40) antibody and common leukocyte antigen CD45 antibody. Detail information of all reagents is specified in Supplementary Table S1. Peptide and controls were mixed at 2× desired concentration in MEB2 buffer +20 μg/mL digitonin (Sigma), and 50 μL of this combination was added per well in a 96-well, non-binding plate (Supplementary Materials and Methods). The cells, in 50 μL MEB2, were added and incubated with the peptides for 1 hour at room temperature and then fixed. Following neutralization, anti–cytochrome C antibody (BioLegend) was added at a 1:2,000 final antibody dilution. Staining was performed at 4°C overnight. Viable D2-40–positive and CD45-negative cells were analyzed by multi-parameter flow cytometry (Attune NxT, Invitrogen). Retained cytochrome C was measured, and percent cytochrome C release was calculated from the mean fluorescence intensity of the cytochrome C stain normalized to that of a well containing 25 μmol/L alamethicin, which serves as 100% release, positive control. For dynamic BH3 profiling (DBP), digested tumor cells were seeded into plates with BH3 mimetics treatment *in vitro*. After 16-hour treatments, the cells were collected for subsequent BH3 profiling analysis. "% Delta priming" refers to the percentage change in mitochondrial priming, calculated by comparing the percentage of cytochrome c loss before and after treatment cells.

Apoptosis analysis

After treatment, cells were stained with annexin V and propidium iodide (PI) according to the manufacturer's instructions. After the cells were incubated at room temperature for 15 minutes in dark, apoptotic cells were analyzed with flow cytometry (Attune NxT, Invitrogen). Apoptotic cell percentage corresponded to annexin V(+)/PI(−) and annexin V(+)/PI(+) cells. Data were analyzed using the FlowJo 10.4.1 software program (Tree Star).

Cell viability assay

The IC_{50} curves were generated by plating 3,000 cells/well in a 96-well plate (Corning). Cells were treated overnight with ABT199 and A1155463 or CDDP was added the next day at the indicated concentrations. Viability was assessed by CellTiter-Glo 2.0 Reagent (Supplementary Materials and Methods). Synergy scoring was determined using the "inhibition readout" on the online SynergyFinder software (https://synergyfinder.fimm.fi; ref. 20) specified in Supplementary Materials and Methods.

Animal studies

All animal experiments were performed in accordance with the Guide for the Care and Use of Laboratory Animals and protocols approved by the Institutional Animal Care and Use Committee of Baylor College of Medicine. Patient-derived xenografts (PDX) were established by the Patient-Derived Xenograft and Advanced *In Vivo* Models core (21). Fresh PDX tumor fragments were transplanted into the cleared, #4 mammary fat pad (right abdominal) of female, 5-week-old NOD/SCID gamma mice [JAX, NOD.Cg-Prkdcscid Il2rgtm1Wjl/SzJ (RRID: BCBC_4611)] and allowed to grow to the study start size of 50 mm^3. The mice were randomized to each treatment groups and were treated with vehicle control, AZD5991, A1155463, AZD5991/A1155463, CDDP, CDDP/AZD5991, A1155364/CDDP, or the combination of three drugs via intraperitoneal injection. The dosage and frequency of drug administration are specified in the figure legends. Body weights and tumor sizes were measured every three days by blinding investigators. Animals were euthanized if (i) tumor volume was ≥1,500 mm^3 and (ii) tumor became ulcerated.

Western blotting

Equal amounts of protein were separated by 4% to 20% SDS-PAGE and were transferred to polyvinylidene fluoride membranes (Millipore). The membranes were incubated overnight at 4°C with primary antibodies at the concentrations specified in Supplementary Table S1. After additional incubation with an anti-immunoglobin horseradish peroxidase–linked antibody for 1 hour, the immune complexes were detected by the SuperSignal West Femto Maximum Sensitivity Substrate (Thermo Fisher Scientific).

Seahorse extracellular flux analysis

Oxygen consumption rates and extracellular acidification rates of cells were measured using a Seahorse Bioscience XF96 Extracellular Flux Analyzer (Supplementary Materials and Methods). Seahorse programing consisted of 3-minute baseline measurements with 1-minute intervals which were repeated after each injection. All values were normalized to DNA content of each well to account for growth differences.

JC-1 assays

Mitochondrial membrane potential ($\Delta\psi m$) changes were detected using the mitochondrial membrane potential–sensitive fluorescent dye JC-1 (Thermo Fisher Scientific) following the manufacturer's instructions. After treatments, the cells were collected and suspended in PBS at approximately 1×10^6 cells/mL containing JC-1 and the cells were incubated at 37°C with 5% CO_2 for 30 minutes. After loading, the cells were washed twice with PBS and analyzed by flow cytometry (Attune NxT, Invitrogen).

Mitochondrial reactive oxygen species detection assay

MitoSOX mitochondrial superoxide indicators (Thermo Fisher Scientific) were used to measure mitochondrial superoxide production within the cell according to the manufacturer's protocol. After treatments, the cells were collected and suspended in PBS at approximately 1×10^6 cells/mL containing indicators and the cells were incubated at 37°C with 5% CO_2 for 1 hour. The cells were then analyzed on a FACS flow cytometer (Attune NxT, Invitrogen). Relative fluorescence intensities were analyzed using FlowJo 10.4.1 software (RRID: SCR_008520).

Immunofluorescence staining

Cells were seeded in Millicell EZ SLIDE four-well glass (Millipore) for immunofluorescence staining according to the protocol. Representative microphotographs were acquired using the EVOS M5000 Imaging System. For high-resolution imaging, the cells were seeded in an ibidi μ-Slide 8 Well high coverslip overnight, and the ONI Discovery Kit (ONI) was used for direct stochastic optical reconstruction microscopy according to the manufacturer's protocol (Supplementary Materials and Methods).

Statistical analysis

Quantitative data are presented as the mean ± SD. The Student *t* test was carried out to compare means between two groups. A one-way ANOVA followed by the *post hoc* Dunnett test was used to compare means of more than two groups, and a multiple range least significant difference was used for intergroup comparisons. For *in vivo* studies, the tumor growth curves were converted to $\log_2$ fold change from baseline and were evaluated using general linear models with random effects to account for mouse within treatment group dependencies. Fold change data at the single time point were simplified to evaluate tumor size changes at a specific time point using repeated-measures ANOVA analyses. Results with $P < 0.05$ were considered statistically significant and are indicated by *, $^{\#}$, $P < 0.05$; and **, $^{\#\#}$, $P < 0.01$. All statistical analyses were performed with SPSS 16.0 (RRID: SCR_002865) and GraphPad.

Data availability

Data related to sensitive patient information have been anonymized to protect privacy and the data generated in this study are available upon reasonable request to the corresponding author.

Results

Dynamics BH3 profiling in diffuse mesothelioma specimens reveals patient-specific responses

Our previous work established that BH3 profiling can identify cell dependence on different antiapoptotic proteins in cultured cell lines as well as fresh EAC and diffuse mesothelioma tumors (7). To assess translational potential and further verify the predictive role of BH3 profiling in patients with diffuse mesothelioma, we generated patient-derived cell (PDC) and PDX models from patient tumor tissue collected at surgery. Four PDCs and one PDX were successfully established. The PDCs had different morphologies, malignant characteristics, cell proliferation rates, colony formation activities, migration, and invasion. Several notable diffuse mesothelioma makers (PanCK, WT-1, D2-40, and CK5/6; ref. 22) were evaluated in PDCs which noted heterogeneity and variability in PDC cell lines (Supplementary Fig. S1). After establishing the PDC and PDX models, we confirmed that the PDC and MPM188 PDX model retained the histologic characteristics of the original tumor (Supplementary Fig. S2; Supplementary Table S3). Next, we performed BH3 profiling on fresh tumor, PDC, and PDX to determine whether BH3 profiles were similar between the models from the same patient (**Fig. 1A**). The binding patterns of BH3 peptides (BIM, BAD, NOXA, MS-1, and HRK) and BH3 mimetics (A1155463, AZD5991, and ABT199) to antiapoptotic proteins (BCL-2, BCL-xL, and MCL-1) were used in the BH3 profiling (**Fig. 1B**). The BH3 profiles of patients with diffuse mesothelioma showed similar activities in the tumor samples 4 hours after surgery compared with both PDC and PDX models (**Fig. 1C**; Supplementary Fig. S3A). For example, one patient strongly responded to MS-1 BH3 peptides in addition to the ubiquitous sensitizer, BIM, in all models, which suggested sensitivity to MCL-1 antagonism (**Fig. 1C**). This prediction was confirmed by noting significant increases in apoptosis with MCL-1 inhibitor, AZD-5991, in combination with CDDP compared with the BCL-2 inhibitor or BCL-xL inhibitor (**Fig. 1D**; Supplementary Fig. S3B). These results show that BH3 profiling is similar across the models and predictive of response to BH3 mimetic treatments.

After verifying the predictive role of BH3 profiling in patients with diffuse mesothelioma, we performed DBP to evaluate whether BH3 mimetics induced mitochondrial apoptotic priming (decreased the threshold to trigger apoptosis) in patients with diffuse mesothelioma (**Fig. 1E**). DBP generates a "delta priming" which is the comparison of BH3 profiles before and after drug treatment (23, 24). Increased priming indicates dependence on corresponding antiapoptotic proteins. We performed DBP in seven patients with diffuse mesothelioma; the heatmap indicated differences in mitochondrial priming between patients. Patients M1207 and MPM196 showed relatively poor priming with BH3 mimetics, whereas patients MPM188 and MPM207 seemed to have a marked response to MCL-1 and BCL-xL inhibition. Furthermore, in all patients treated with BH3 mimetics, we noticed that

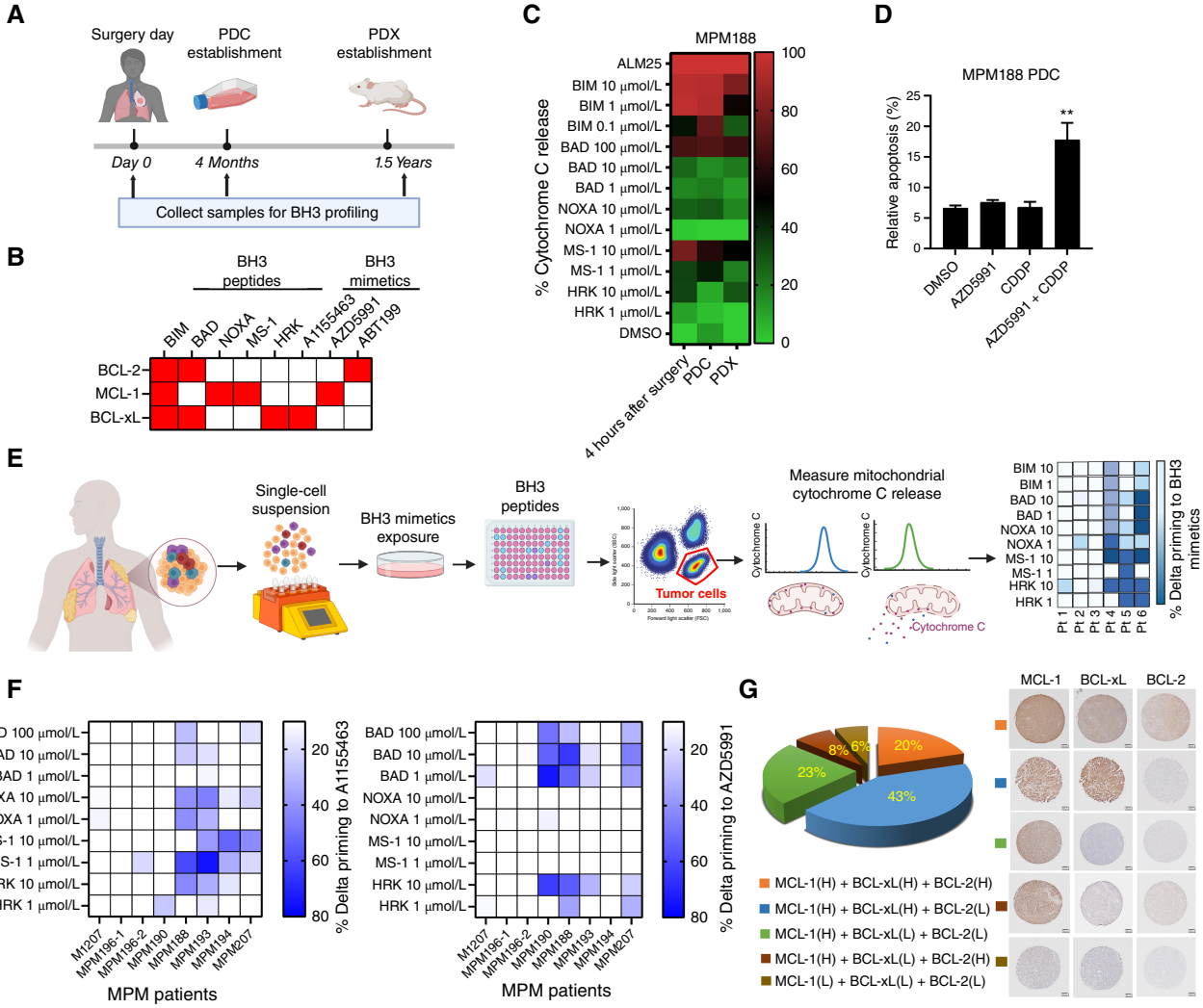

Figure 1.

Dynamic BH3 profiling in diffuse mesothelioma specimens reveals patient-specific responses. **A,** Timeline of BH3 profiling in fresh samples from patients with diffuse mesothelioma, diffuse mesothelioma–derived cells (PDCs), and xenografts (PDXs). **B,** Interaction map for BH3 peptides and BH3 mimetics with BCL-2 family proteins. Red indicates high-affinity binding and white indicates low-affinity binding. **C,** Heatmap showing BH3 profiling in MPM188 patient samples at 4 hours compared with PDC and PDX when exposed to the indicated peptides. Data were normalized to DMSO (as negative control) and alamethicin (ALM25, as positive control). **D,** After pretreatment with 1.0 μmol/L AZD5991 for 24 hours, the apoptotic ratio in cells at 48 hours after treatment with CDDP was measured by annexin V flow cytometry; cells positive for annexin V staining were counted as apoptotic cells (**, $P < 0.01$ for treatment vs. DMSO). **E,** The workflow for measuring BH3 mimetics–induced priming using DBP on primary samples from patients with diffuse mesothelioma. **F,** Heatmap of mitochondrial priming of fresh samples with 1.0 μmol/L AZD5991 or A1155463 treatment for 16 hours. **G,** The expression profiles of MCL-1, BCL-xL, and BCL-2 in each case are shown as a percentage of all 50 cases. (H) or (L) means high or low expression, respectively. Representative images of IHC expressions of MCL-1, BCL-xL, and BCL-2 in tissue microarray from patients with diffuse mesothelioma. (**A** and **E,** Created in BioRender. https://BioRender.com/a478jgq, https://BioRender.com/8wvjw5w, and https://BioRender.com/t7qk0fq.)

the MCL-1 sensitizers, NOXA and MS-1 peptides, were most responsive when treated with the BCL-xL inhibitor, A1155463. Additionally, when treated with the MCL-1 inhibitor AZD5991, the peptides BAD and HRK were increased, which suggests that these tumors are now responsive to BCL-xL (**Fig. 1F**). These results suggested that BCL-xL and MCL-1 have functional redundancy in which they play compensatory roles for each other. In other words, when treating MCL-1, BCL-xL increases as a compensatory mechanism to prevent induction of apoptotic pathways.

To further investigate clinical importance of Bcl-2 proteins, we assessed the expression profiles of MCL-1, BCL-xL, and BCL-2 in a tissue microarray. High MCL-1 expressions were found in 88 of 94 cases (93%), high combination of MCL-1, BCL-xL, and BCL-2 expressions was observed in 19 of 94 cases (20%), and high BCL-xL and MCL-1 were observed in 40 of 94 cases (43%). The MCL-1^{high}/BCL-xL^{high} population (63%) was the most common profile in diffuse mesothelioma (**Fig. 1G**). These results suggest that targeting both MCL-1 and BCL-xL may be a treatment strategy for patients with diffuse mesothelioma.

Synergistic cell death is induced by the combination of MCL-1 and BCL-xl inhibition in diffuse mesothelioma cell lines

Most solid tumors are not sensitive to single-agent treatment with BH3 mimetics (10, 23, 25–27). We previously reported that S63845 (previously used agent), ABT199 (targeting BCL-2), and A1155463 (targeting BCL-xL) had weak activity on EAC and diffuse mesothelioma cells (7). We extended these findings to additional diffuse mesothelioma cell lines, as well as diffuse mesothelioma PDC. As expected, all cells were relatively resistant to single-agent AZD5591, A1155463, and ABT199 (**Fig. 2A**). Given that MCL-1 and BCL-xL are co-expressed in diffuse mesothelioma, we treated the cell lines, H28 and H2452, and PDC to evaluate the cytotoxic activity of AZD5991 in combination with titrated, non-sensitizing concentrations of A1155463. Cell death was observed with A1155463 with IC_{50} values 60- to 200-fold less than single agents in diffuse mesothelioma cells (Supplementary Fig. S4A). The combination treatment resulted in

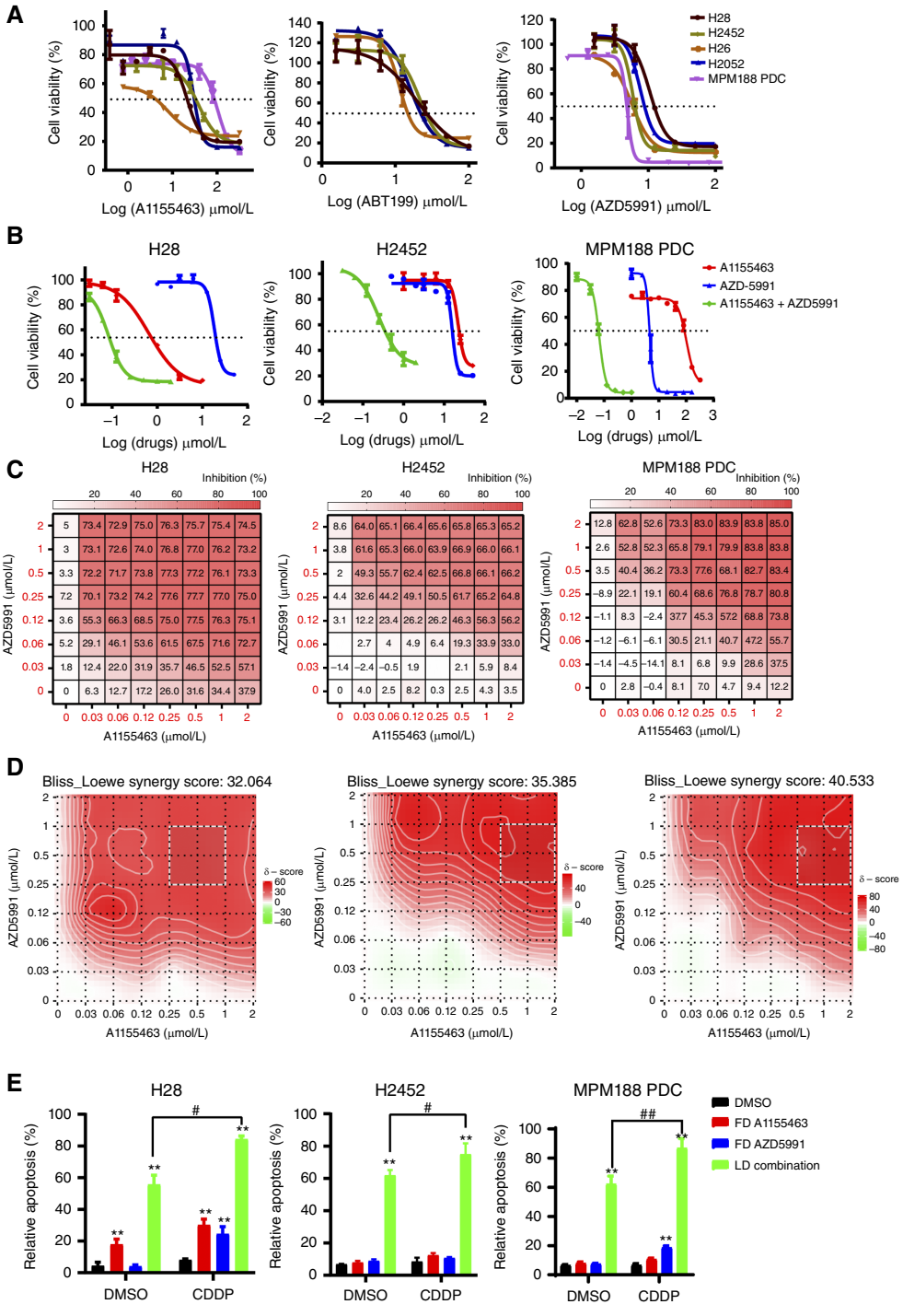

Figure 2.

Synergistic cell death is induced by the MCL-1 inhibitor, AZD5991, and BCL-xL inhibitor, A1155463, in diffuse mesothelioma cell lines. **A,** Single-agent activity of BH3 mimetics in diffuse mesothelioma cell lines after 48 hours of treatment. The IC_{50} values of AZD5991, A1155463, and ABT199 were calculated. Data are presented as mean ± SD of four technical replicates from three independent experiments. **B,** Cell death was assessed upon exposure of diffuse mesothelioma cell lines to increasing concentrations of AZD5991 and/or A1155463 for 48 hours. Data are presented as mean ± SD of three technical replicates from three independent experiments. **C,** The heatmaps showing dose–response matrix analyses based on cell death with the MCL-1 inhibitor, AZD5991, and BCL-xL inhibitor, A1155463. **D,** Visualization of the calculated 2D synergy maps for the cell viability assay from the SynergyFinder Bliss_Loewe independence model combinatorial analysis. Red regions represent synergy and green regions represent antagonism. **E,** After pretreatment with FD 1.0 μmol/L AZD5991 or FD 1.0 μmol/L A1155463 and the combination of LD 0.1 μmol/L AZD5991 and LD 0.1 μmol/L A1155463 for 24 hours, the apoptotic ratio in cells at 48 hours after treatment with CDDP was measured by annexin V flow cytometry; cells positive for annexin V staining were counted as apoptotic cells (**, $P < 0.01$ for treatment vs. DMSO; #, $P < 0.05$ for combination treatment vs. A1155463 and AZD5991 co-treatment; ##, $P < 0.01$ for combination treatment vs. A1155463 and AZD5991 co-treatment.)

significant cytotoxicity in insensitive cells with either treatment alone (**Fig. 2B**; Supplementary Fig. S4B). With the SynergyFinder program, we assessed AZD5991 and A1155463 combinations and observed a distribution that confirmed the predictive, synergistic effects in the region around IC_{50}. These results are based on synergy scores over 10, which are considered synergistic. The most synergistic area was 0.125 to 0.5 μmol/L, which showed about 80% inhibition with a score around 30 (**Fig. 2C** and **D**; Supplementary Fig. S4C). Based on these results, we chose 0.1 μmol/L as the combination dose for future studies. In our previous work, we found that targeting MCL-1 or BCL-xl with S63845 or A1155463 in combination with CDDP significantly increased apoptosis compared with CDDP alone (7). To determine whether the redundancy of MCL-1 and BCL-xl reduced the synergistic effects of either agent alone with CDDP, we treated cells with the combination of AZD5991 and A1155463 with CDDP. We observed that targeting both MCL-1 and BCL-xL significantly increased apoptosis with CDDP (**Fig. 2E**; Supplementary Fig. S4D). Hence, these data demonstrate that co-targeting BCL-xL and MCL-1 may block the compensatory mechanisms of Bcl-2 antiapoptotic proteins to synergistically increase apoptosis and enhance chemotherapy response.

MCL-1 inhibition enhances antitumor response of CDDP in PDX models

We evaluated AZD5991 and A1155463 in the MPM188 PDX model. First, we performed a tolerance study in non–tumor-bearing NOD/SCID gamma mice with AZD5991 at 0.5 mg/kg to 10 mg/kg and A1155463 at 0.25 mg/kg to 5 mg/kg. We found that the combination of MCL-1 and BCL-xL at lower doses was well tolerated based on stable body weight (**Fig. 3A**). In contrast, higher doses were lethal within 5 hours even though the single agents were well tolerated at the same dose.

Next, we performed an efficacy *in vivo* experiment. Mice bearing MPM188 tumors were randomized into eight arms with vehicle, full-dose (FD) AZD5991, FD A1155463, FD AZD5991, or FD A1155463 with CDDP, and low dose (LD) with and without CDDP (**Fig. 3B**). FD AZD5591 and FD A1155463 as single agents, as well as the LD combination of AZD5991 and A1155463, did not result in significant tumor growth inhibition consistent with our *in vitro* results. In contrast, single-agent FD AZD5991 with CDDP significantly reduced tumor growth. Treatment with FD A1155463 also resulted in significant growth inhibition; however, A1155463 was less effective than AZD5991 (**Fig. 3C** and **D**; Supplementary Table S4). We confirmed the enhanced efficacy of the single-agent FD AZD5991 with CDDP by the mass of tumors collected on day 78 when the vehicle group reached endpoint; the slight tumor suppression effects observed with the triple combination treatment compared with single-agent treatments were attributable to the low combination doses used, which, although synergistic *in vitro*, may not reach optimal therapeutic efficacy *in vivo* at these safety levels (**Fig. 3E**). Moreover, AZD5991 with CDDP significantly increased survival compared with vehicle or single-agent treatments (**Fig. 3F**). Importantly, body weight remained constant during the *in vivo* study period and mice seemed healthy after treatment. These data suggested that MCL-1 inhibition increases mitochondrial priming to enhance the chemosensitivity to CDDP in diffuse mesothelioma.

We performed DBP on harvested mouse tumors and compared each treatment arm with control to identify antiapoptotic dependency changes. The PDX tumors treated with AZD5991 and CDDP had the most growth inhibition, which was consistent with the greatest change in the DBP. In contrast, the DBP showed almost no priming in the LD combination group which is consistent with a lack of tumor response. AZD5991 or CDDP showed significantly increased response to MS-1, BAD, and NOXA BH3 peptides, indicating an increased dependency to MCL-1, whereas an increase in the HRK BH3 peptide suggests that MCL-1 antagonism also drives BCL-xL dependency (**Fig. 3G**). Our results are consistent with prior reports that DBP measures early changes in apoptotic signaling which occur before frank apoptosis (28). These data confirm that BCL-xL and MCL-1 have compensatory roles in antitumor effects, antagonizing results of increased dependence on the other.

Co-targeting MCL-1 and BCL-xL synergistically increases cell death through the intrinsic mitochondrial apoptotic pathway

We evaluated whether co-targeting BCL-xL and MCL-1 synergistically increases cell death via the mitochondrial apoptotic pathways. We knocked down MCL-1 and BCL-xL (shMCL-1 and shBCL-xL) to determine whether these knockdowns phenocopied pharmacologic inhibition. First, H28 and H2452 cells did not survive double knockdown of MCL-1 and BCL-xL. Interestingly, the protein expression of MCL-1 was significantly elevated in shBCL-xL H28 and H2452 cells, whereas shMCL-1 had no effect on BCL-xL expression. BCL-2 expression did not have a consistent pattern in either H28 or H2452 cell lines with MCL-1 and BCL-xL knockdowns (**Fig. 4A**). Our previous study found that mesothelioma has a lower dependence on Bcl-2 for survival and is less sensitive to its targeted inhibition by ABT199 (7). Therefore, in this study, we did not explore the ABT199 efficacy in mesothelioma. Next, we treated shMCL-1 cells with the BCL-xL inhibitor A1155463 and shBCL-xl cells with the MCL-1 inhibitor AZD5991. shMCL-1 sensitized the cells to A1155463; similarly, shBCL-xL sensitized the cells to AZD5991 (**Fig. 4B**). Significantly increased apoptosis was observed in shMCL-1 or shBCL-xL cells with the drug targeting the other protein (**Fig. 4C**). These results are consistent with the synergistic effects of dual pharmacologic inhibition of MCL-1 and BCL-xL.

MCL-1 and BCL-xL exert antiapoptotic activity by inhibiting the effector proteins of MOMP called BAX and BAK (3). To verify on-target engagement of MOMP when co-targeting MCL-1 and BCL-xL, we knocked down BAX and BAK ($DKD^{bax/bak}$; **Fig. 4D**). The $DKD^{bax/bak}$ cells were significantly more resistant to AZD5991 and A1155463, with 60% of shCTL cells exhibiting apoptosis compared with less than 20% of $DKD^{bax/bak}$ (**Fig. 4F**). We repeated the experiments in PDCs (MPM188 and MPM193) and noted similar findings that blocking MOMP by $DKD^{bax/bak}$ prevented synergistic cell death when co-targeting MCL-1 and BCL-xL (Supplementary Fig. S5).

BCL-xL inhibition induced mitochondrial damage and dysfunction

MCL-1 and BCL-xL maintain mitochondrial integrity and dynamics (29–32). To investigate whether MCL-1 and BCL-xL play contributing roles in mitochondrial integrity and dynamics during treatment-induced cell death, we assessed mitochondrial changes in H28 and H2452 cells. To assess morphology, we performed direct stochastic optical reconstruction microscopy to observe mitochondria ultrastructural changes at super resolution (33). Cells were labeled with a mitochondrial marker TOM20. We observed reticulated and elongated mitochondria in shCTL and shMCL-1 cells. In contrast, the mitochondria were fragmented and almost exclusively perinuclear in shBCL-xL cells (**Fig. 5A**). Similarity, A1155463 induced markedly perinuclear clustering of mitochondria unlike AZD5991. Additionally, H28 and H2452 cells

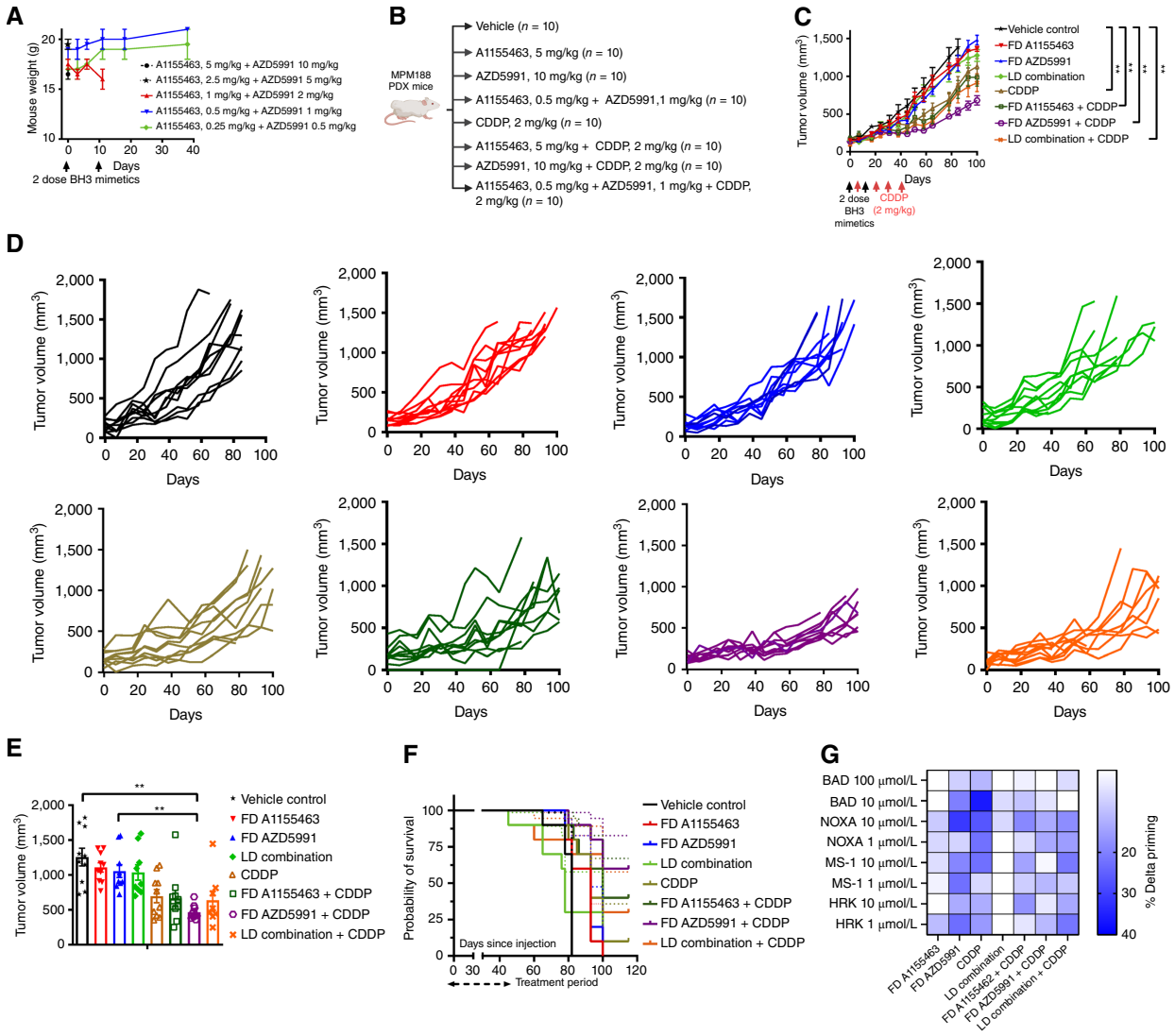

Figure 3.

MCL-1 inhibitor AZD5991 enhances antitumor response of CDDP in the MPM188 PDX model. **A,** Changes of mouse body weight upon treatment with different combinational concentrations of AZD5991 and A1155463. **B,** Groups of mice for the experiment. Once the tumor volume reached between 50 and 100 mm^3, the mice were randomized to each treatment or control group and were treated with vehicle control, FD AZD5991 (10 mg/kg), FD A1155463 (5 mg/kg), LD AZD5991 (1 mg/kg), LD A1155463 (0.5 mg/kg), CDDP (2 mg/kg), the combination of FD AZD55991 and CDDP, combination of FD A1155364 and CDDP, or the combination of LD AZD5991 and LD A1155463 with CDDP via intraperitoneal injection. **C,** Cumulative graph of mean tumor size (mm^2) per group. (**, $P < 0.01$ for treatments vs. vehicle control). **D,** Tumor size (mm^2) of individual mice in each group from experiment described in **B**. **E,** Tumor masses on day 78 (the day that vehicle group reached endpoint). Each point is the mass of an individual tumor with the bar indicating the mean ± SD ($n = 10$). (**, $P < 0.01$ for combination treatment vs. single AZD5991 treatment or vehicle control). **F,** Kaplan–Meier survival curves with log-rank analysis of mice treated with different groups, with relevant vehicle controls. The survival endpoint was when tumors reached a volume of 1,500 mm^3 as dictated by the ethics approval associated with this experiment. **G,** Heatmap of mitochondrial priming was generated by comparison of BH3 profiles of PDX samples from vehicle control groups between each treatment arms.

with LD AZD5991 and A1155463 combination showed the presence of punctate-like mitochondria throughout the cytoplasm (**Fig. 5B**). Mitochondrial fragmentation results in loss of fusion or increase in fission. However, we did not observe consistent changes of mitochondrial fission (Drp1 and FIS1) and fusion (MFN1 and MFN2) proteins after the inhibition of MCL-1 or BCL-xL *in vitro* or *in vivo* (Supplementary Fig. S6). These results suggest that the synergistic effects of MCL-1 and BCL-xL on tumor cell death are not mediated via fusion or fission.

Given that mitochondrial clustering coinciding with nuclear fragmentation is potentially a distinct feature of cells with dysfunctional mitochondria (34, 35) and that we observed that targeting BCL-xL led to marked perinuclear clustering of mitochondria, we investigated the effects of BCL-xL and MCL-1 on the mitochondrial metabolic status by measuring oxidative phosphorylation. Seahorse data showed that shBCL-xL resulted in significant decreases in ATP production, basal respiration, and maximal respiration compared with shMCL-1 and shCTL in

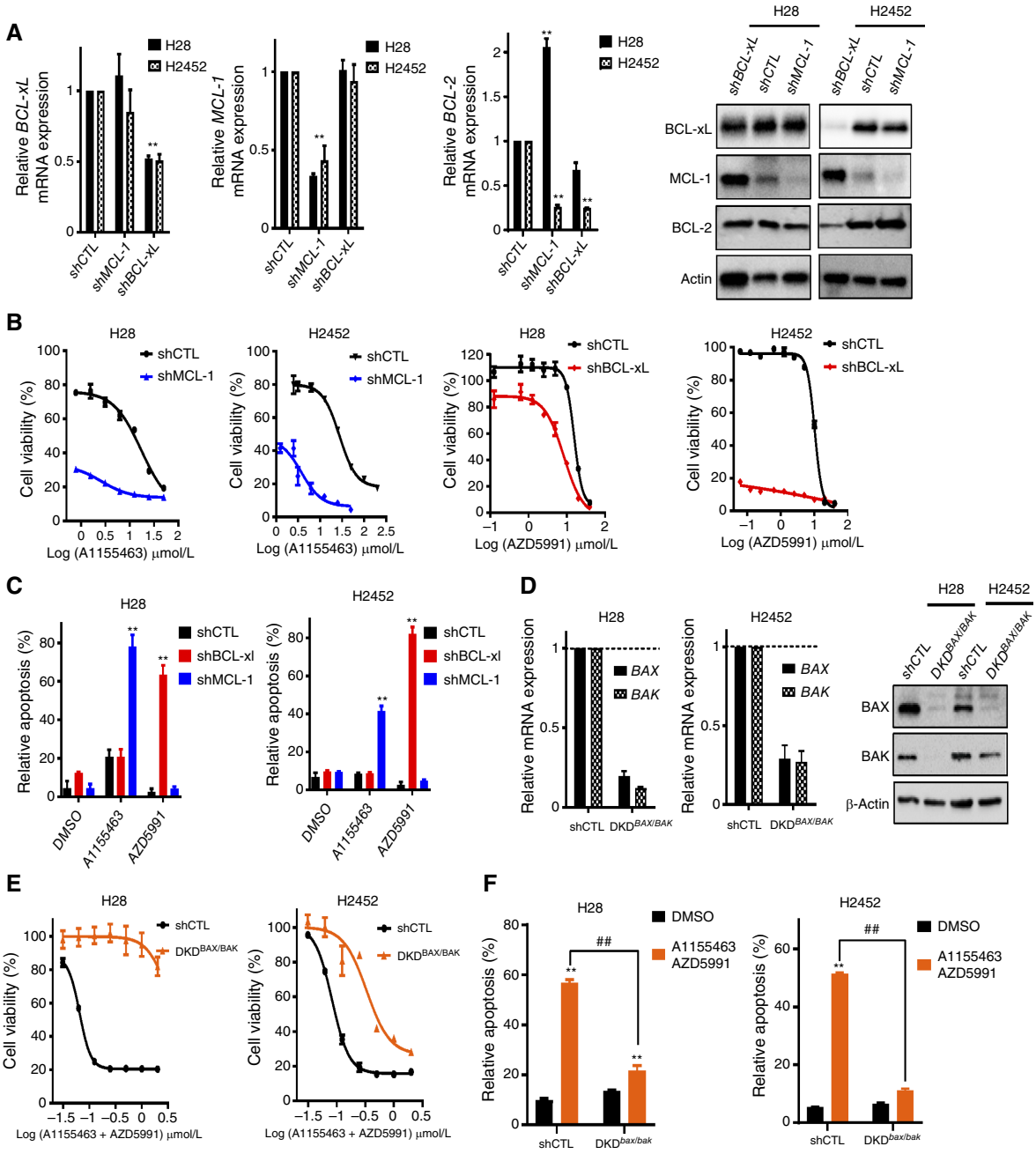

Figure 4.

Co-targeting MCL-1 and BCL-xL synergistically increases cell death through the intrinsic mitochondrial apoptotic pathway in diffuse mesothelioma cell lines. **A,** Stable knockdown of MCL-1 (shMCL-1), BCL-xL (shBCL-xL), or scrambled control (shCTL) was generated in H28 and H2452 cells by transfecting short hairpin RNA lentiviruses. The mRNA and protein levels of MCL-1, BCL-xL, and Bcl-2 were analyzed by qRT-PCR analysis and Western blotting. **B,** Cell viability at 48 hours in shCTL, shMCL-1, and shBCL-xL cell lines treated with either AZD5991 or A1155436 alone. The IC_{50} values of AZD5991 and A1155463 were determined in different condition cells. Data are mean ± SD of four technical replicates from three independent experiments. **C,** After pretreatment with 1.0 μmol/L FD AZD5991 or 1.0 μmol/L FD A1155463, the apoptotic ratio in shCTL, shMCL-1, and shBCL-xL cells was measured by annexin V flow cytometry; cells positive for annexin V staining were counted as apoptotic cells (**, $P < 0.01$ for treatment vs. DMSO in respective cells). **D,** Stable double knockdown of Bax and Bak ($DKD^{bax/bak}$) or scrambled control (shCTL) was generated in H28 and H2452 cells by transfecting short hairpin RNA lentiviruses. The mRNA and protein levels of Bax and Bak were analyzed by qRT-PCR analysis and Western blotting. **E,** Cell viability at 48 hours in shCTL and $DKD^{Bax/Bak}$ cell lines when treated with the combination of AZD5991 and A1155463. The IC_{50} values of AZD5991 and A1155463 were determined in different conditions. Data are mean ± SD of four technical replicates from three independent experiments. **F,** After pretreatment with the combination of LD AZD5991 and A1155463 for 24 hours, the apoptotic ratio in shCTL and $DKD^{Bax/Bak}$ cells was measured by annexin V flow cytometry; cells positive for annexin V staining were counted as apoptotic cells (**, $P < 0.01$ for treatment vs. DMSO, ##, $P < 0.01$ for $DKD^{Bax/Bak}$ vs. scrambled control).

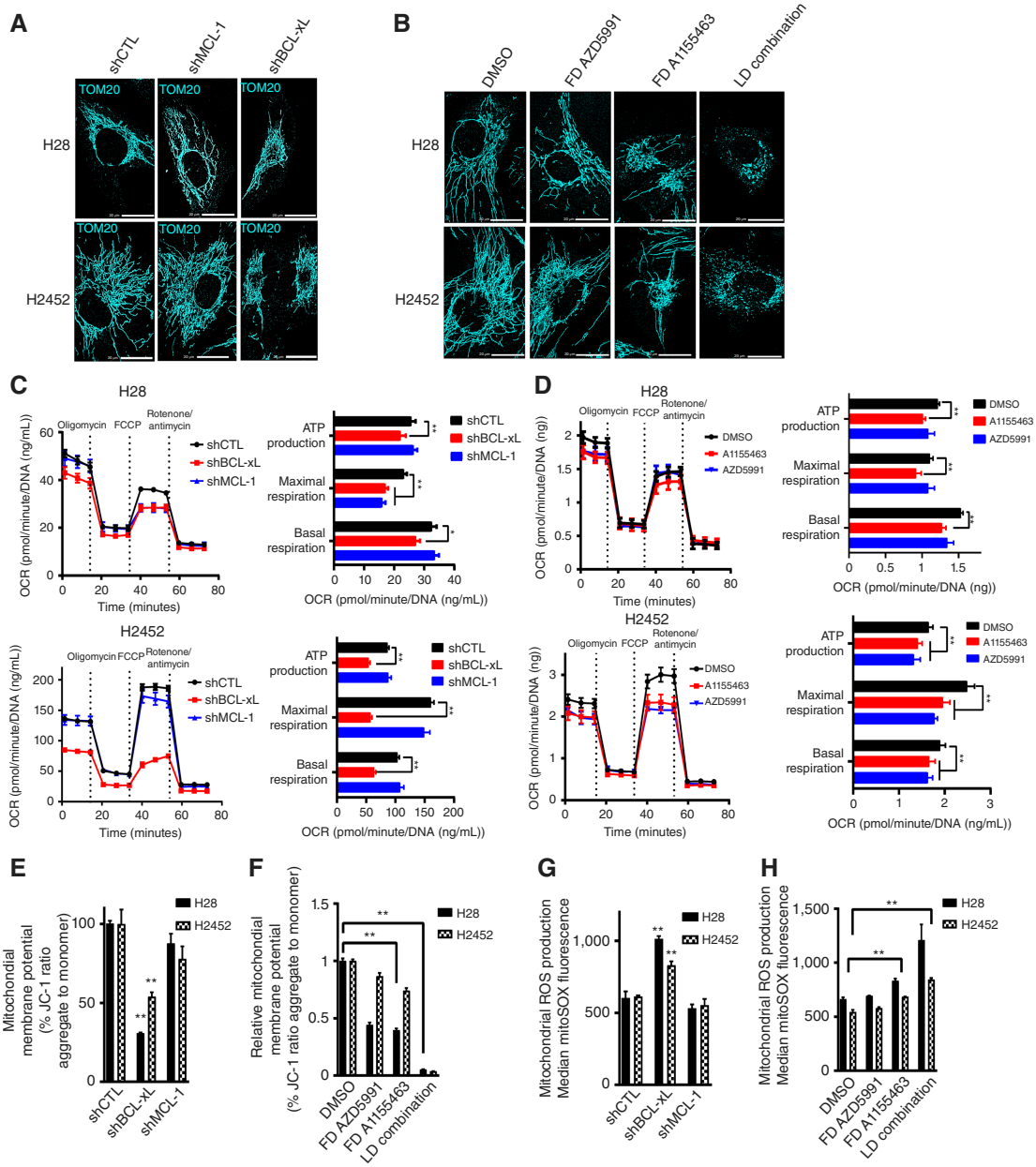

Figure 5.

BCL-xL inhibition induced mitochondrial damage and dysfunction in diffuse mesothelioma cell lines. **A,** Representative **s**uper-resolution imaging of mitochondria labeled with TOM20 in shCTL, shMCL-1, and shBCL-xL cell lines. Scale bar, 20 μm. **B,** Representative super-resolution imaging of mitochondria labeled with TOM20 in H28 and H2452 cells with FD AZD5991, FD A1155463, and LD combination of AZD5991 and A1155463 treatments for 24 hours. Scale bar, 20 μm. **C,** Oxygen consumption rate was measured with sequential injections of oligomycin, FCCP, and rotenone/antimycin at the time points indicated in shCTL, shMCL-1, and shBCL-xL in H28 and H2452 cell lines. Basal respiratory capacity, maximal respiration, and ATP production were calculated as described in the Supplementary Materials and Methods section. **D,** After treatment with FD AZD5991, FD A1155463, or the combination of LD AZD5991 and A1155463 for 24 hours, the OCR was measured with sequential injections of oligomycin, FCCP, and rotenone/antimycin at the time points indicated in H28 and H2452 cell lines. **E,** Analysis of mitochondrial membrane potentials (ΔΨm) using flow cytometry with JC-1 dye in shCTL, shMCL-1, and shBCL-xL in H28 and H2452 cell lines. Loss of ΔΨm was demonstrated by the change in JC-1 fluorescence from red (JC-1 aggregates) to green (JC-1 monomers) represented as the ratio of JC-1 red to green fluorescence in different conditional cells (**, $P < 0.01$ compared with indicated control groups). **F,** After treatment with FD AZD5991, FD A1155463, or the combination of LD AZD5991 and A1155463 for 24 hours, mitochondrial membrane potentials (ΔΨm) were measured using flow cytometry with JC-1 dye in H28 and H2452 cell lines (**, $P < 0.01$ compared with indicated control groups). **G,** Mitochondrial reactive oxygen species concentrations were measured using MitoSOX Red reagent by flow cytometry with the median of fluorescence ±SD analyzed using FlowJo software in shCTL, shMCL-1, and shBCL-xL in H28 and H2452 cell lines. (**, $P < 0.01$ compared with indicated control groups). **H,** After treatment with FD AZD5991, FD A1155463, or the combination of LD AZD5991 and A1155463 for 24 hours, mitochondrial reactive oxygen species concentrations were measured using MitoSOX Red reagent by flow cytometry with the median of fluorescence ±SD analyzed using FlowJo software in conditional H28 and H2452 cells (**, $P < 0.01$ compared with indicated control groups). OCR, oxygen consumption rate; ROS, reactive oxygen species.

H2452 cells (**Fig. 5C**). Similarly, we observed lower decreased oxygen consumption rates in cells with the BCL-xL inhibitor A1155463 (**Fig. 5D**). Oxidative phosphorylation deficiency reduces mitochondrial membrane potential (Δψm) with concomitant increases in reactive oxygen species (36, 37). We observed that inhibition of BCL-xL decreased mitochondrial membrane potential by JC-1 (**Fig. 5E**). Similar changes were observed with pharmacologic inhibition of BCL-xL (**Fig. 5F**). Meanwhile, we found that genetic or pharmacologic inhibition of BCL-xL induced mitochondrial superoxide production compared with MCL-1 inhibition (**Fig. 5G** and **H**). These observations suggest that BCL-xL inhibition impaired mitochondrial respiration, increased mitochondrial reactive oxygen species production, and enhanced mitochondrial membrane damage leading to mitochondrial dysfunction, whereas MCL-1 inhibition did not show similar toxic effects on the mitochondria.

BCL-xL inhibition induced MCL-1 accumulation in mitochondria

Given that shBCL-xL significantly increases MCL-1 levels (**Fig. 4A**) and co-targeting BCL-xL and MCL-1 synergistically increases cell death (**Fig. 2B**; ref. 30), we hypothesized that cell death with BCL-xL inhibition was protected by the increase in MCL-1 protein expression on the mitochondrial membrane and, thus, these cells were particularly vulnerable to MCL-1 inhibition. We investigated the localization of MCL-1 in shBCL-xl cells by immunofluorescence and observed MCL-1 accumulation localized to the mitochondria in shBCL-xL cells (**Fig. 6A**). We confirmed this by mitochondrial and cytosolic protein extraction (**Fig. 6B**). Similarly, mitochondrial accumulation of MCL-1 was observed in H28 and H2452 cells when treated with the BCL-xL inhibitor A1155463; MCL-1 was overexpressed after AZD5991 treatments, and the majority MCL-1 protein increases in cytosolic fraction

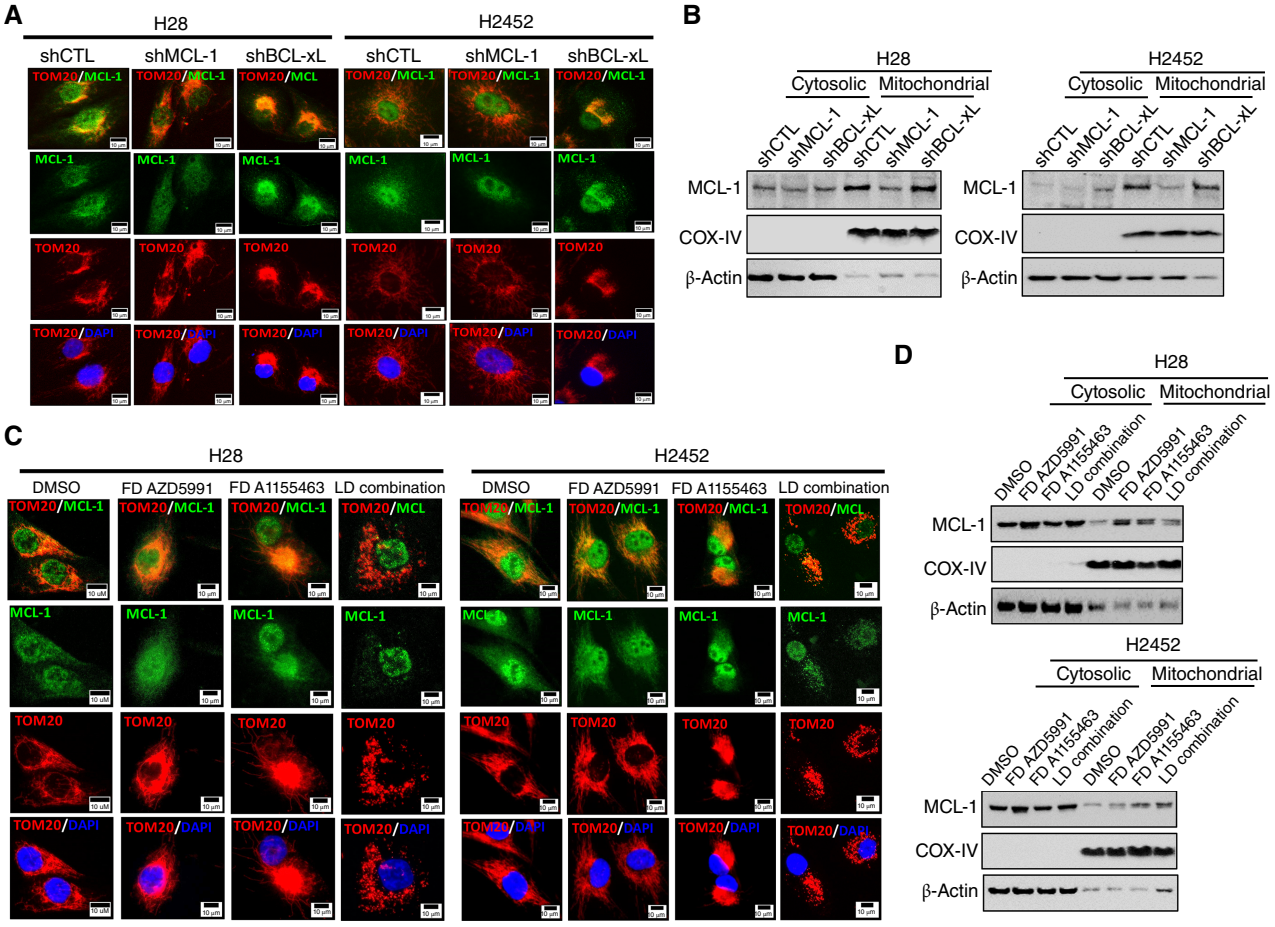

Figure 6.

BCL-xL inhibition induced MCL-1 translocation to mitochondria in diffuse mesothelioma cells. **A,** Colocalization between mitochondria and MCL-1 was assessed in shCTL, shMCL-1, and shBCL-xL H28 and H2452 cell lines by immunofluorescence staining of TOM20 (red), MCL-1 (green), and the nucleus by DAPI (blue). Scale bar, 10 μm. **B,** Immunoblots for MCL-1 were performed on the mitochondrial and cytosolic fractions in shCTL, shMCL-1, and shBCL-xL H28 and H2452 cell lines. Separation of mitochondria and cytosol was controlled using COX-IV and β-actin, respectively. **C,** H28 and H2452 cells were used to assess the mitochondrial integrity and colocalization with MCL-1 after FD AZD5991, FD A1155463, or LD combination of AZD5991 and A1155463 for 24 hours by immunofluorescence staining of TOM20 (red), MCL-1 (green), and the nucleus by DAPI (blue). Scale bar, 10 μm. **D,** H28 and H2452 cells were treated with FD AZD5991, FD A1155463, or LD combination of AZD5991 and A1155463 for 24 hours. Immunoblots for MCL-1 were performed on the mitochondrial and cytosolic fractions in different conditions-treated H28 and H2452 cells. Separation of mitochondria and cytosol was controlled using COX-IV and β-actin, respectively.

with AZD5991 treatments (**Fig. 6C** and **D**) blocked MCL-1 ubiquitination via enhanced deubiquitination to increase MCL-1 protein stability (38). Additionally, in H28 and H2452 cells treated with LD AZD5991 and A1155463, highly fragmented and dispersed mitochondria with lower levels of MCL-1 were noted, which confirms that the mitochondria are highly damaged by the combination treatment. This mitochondrial impairment likely contributes to the synergistic effects on cell death.

Discussion

BH3 profiling is a functional predictive biomarker for BH3 mimetic treatment (6, 23, 28, 39). However, BH3 profiling to rapidly and directly assess the drug responsiveness in patients' fresh primary tumors is limited. In this project, we evaluated whether BH3 profiles are consistent from the same patient samples in fresh tumor after 4 hours, in PDC after 3 months in culture, and in PDX developed over 1.5 years. Importantly, we observed similar BH3 profiles in all models. For example, we noted similarities in response to BAD and MS-1 peptides in fresh tumor, as well as PDX. The adaptation during long-term *ex vivo* culture alters drug sensitivity compared with fresh tumor; our results suggest that BH3 profiles, which measure real-time mitochondrial protein interactions, remain stable over time. These findings enable mechanistic studies on long-term PDC and PDX models to further investigate results derived from fresh tumor. Ultimately, the goal is to perform DBP as a predictive assay of drug response within days of biopsy to guide precision-based treatment decisions in each patient. To date, DBP has not been performed to change clinical decisions. Our results will help validate that findings in long-term models may be applicable to results obtained within hours of biopsy.

BCL-xL and MCL-1 are important in diffuse mesothelioma as noted in our cell line and tissue microarray data (40, 41). We previously demonstrated that inhibiting either BCL-xL or MCL-1 alone had limited impact on cell death (7); we verified that targeting MCL-1 or BCL-xL as single agents in PDX models had minimal efficacy consistent with others' work (41, 42). Given that MCL-1 and BCL-xL exhibit functional redundancy, we evaluated whether dual inhibition is a more effective strategy. Recently, many groups showed that co-targeting BCL-xL and MCL-1 is highly effective in a variety of tumors (9, 43). Ryan and colleagues (26) performed a drug screen in 10 tissue types with a combination of selective BCL-2, BCL-xL, and MCL-1 inhibitors and discovered that most cell lines displayed synergistic dependence on BCL-xL and MCL-1. Similarly, co-targeting MCL-1 and BCL-xL resulted in reduced cell viability of cells from head and neck squamous cell carcinoma (44). BCL-xL antagonism was reported to sensitize diffuse mesothelioma cell lines to MCL-1 inhibition (23, 40). Others report that RNAi against MCL-1 and BCL-xL induces diffuse mesothelioma cell death (45). Our data also showed that combinational treatment with A1155463 and AZD5991 induced rapid and almost 100% cell death in diffuse mesothelioma cell lines and PDC. However, toxicity may limit clinical implementation. We found that the combination of MCL-1 and BCL-xL inhibitors was rapidly lethal in mice within 5 hours. Other groups have observed the same effects (23). We decreased the dose by a factor of 10 and noted that all mice tolerated the treatment but had almost no antitumor efficacy. Other groups have shown that the dosing schedule of navitoclax and S63845 can overcome toxicity and maintain antitumor efficacy (6, 9). Another group tried to avoid the off-target effects of BCL-xL inhibition in the human hematopoietic system and of MCL-1 inhibition in cardiac toxicity by using very low doses of S63845 and A1331852 (10). Regardless, titrating to a safe therapeutic window will be challenging and may limit clinical development.

MCL-1 and BCL-xL have functions beyond apoptosis. MCL-1 regulates the mitochondrial inner membrane–mediated fission by enhancing its ability to antagonize cell death (46, 47). BCL-xL prevents loss of outer membrane integrity to maintain mitochondrial metabolite exchanges by preventing membrane hyperpolarization and mitochondrial swelling in response to a diverse set of stimuli (31, 48). We found that BCL-xL inhibition induced mitochondrial morphology changes and perinuclear clustering. These phenotypes were not observed when targeting MCL-1 which indicates that mitochondrial homeostasis is less dependent on MCL-1 and that BCL-xL has potential functions other than the canonical apoptosis. These findings are supported by inconsistent changes of mitochondrial fission (Drp1 and FIS1) and fusion (MFN1 and MFN2) proteins with MCL-1 inhibition. MCL-1 maintains mitochondrial homeostasis by interactions with DRP-1 and OPA1, which are essential regulators of mitochondrial morphology and dynamics (46, 49). Therefore, blocking MCL-1 may result in the inability to alter mitochondrial dynamics. Alternatively, MCL-1 is localized to distinct mitochondrial sub-compartments that alter mitochondrial activity and integrity (30, 50). Regardless, MCL-1 exerts its antiapoptotic activity on the outer mitochondrial membrane in which it antagonizes BAX and BAK activation which is critical to chemosensitization (51).

Our data show that high levels of MCL-1 are present on the mitochondria after BCL-xL inhibition which is likely required to maintain mitochondrial integrity. This integrity is lost with inhibition of both MCL-1 and BCL-xL, which may explain the lethality of this approach. Moreover, we found that BCL-xL inhibition impaired mitochondrial respiration and decreased mitochondrial membrane potential. Blocking BCL-xL likely enables opening of permeability transition pores on the mitochondrial membrane by increasing Ca^{2+} accumulation in the mitochondrial matrix (48). Based on other reports and our data showing that knockdown of BCL-xL significantly increases MCL-1 levels in mitochondria, we speculate that BCL-xL inhibition through its canonical apoptotic and emerging non-apoptotic roles impairs mitochondrial dysfunction by directly inducing depolarization and energy loss, resulting in increased MCL-1 dependency. Our results reveal that mitochondrial fragmentation with BCL-xL inhibition supports this mechanism.

Collectively, we found that BH3 profiling served as a live cell, predictive bioassay to identify patient responses to treatments, which has high potential for near-term translation to the clinic. Furthermore, we found that dual inhibition of MCL-1 and BCL-xL is synthetically lethal and not a safe treatment strategy. However, the FDA placed the clinical hold on Mcl-1 inhibitor AZD5991 (NCT03218683) and AMG 397 (NCT03465540) following cardiac toxicity (52). In addition to the on-target thrombocytopenia from BCL-xL, our study shows that BCL-xL inhibition induces mitochondrial dysfunction through non-apoptotic on-target effects. However, MCL-1 inhibition seems safe and efficacious when combined with standard chemotherapy but may not be tolerated with another Bcl-2 inhibitor. These findings may lead to the re-emergence of MCL-1–targeting agents in clinical use.

Authors' Disclosures

R.T. Ripley reports grants from NIH, Roderick D. MacDonald Research Fund, and Michael E. DeBakey Department of Surgery Faculty Research Award during the conduct of the study. Y. Xu reports grants from NIH, Roderick D. MacDonald

Research Fund, and Michael E. DeBakey Department of Surgery Faculty Research Award during the conduct of the study. C.G. Medina reports grants from NIH, Michael E. DeBakey Department of Surgery Faculty Research Award, and Roderick D. MacDonald Research Fund at Baylor St. Luke's Medical Center during the conduct of the study. L.E. Dobrolecki reports grants from Cancer Prevention and Research Institute of Texas during the conduct of the study, as well as personal fees from StemMed, Ltd. outside the submitted work. M. Vilchis reports grants from NIH and Baylor St. Lukes Medical Center during the conduct of the study. S.G. Hilsenbeck reports grants from NIH during the conduct of the study. N. Li reports grants from the NIH R03 Award (R03 CA252685-01), the NIH R21 Award (R21 CA256466), NIH R37 Award (R37 CA289419), Michael E. DeBakey Department of Surgery Faculty Research Award, and Roderick D. MacDonald Research Fund at Baylor St. Luke's Medical Center. J.C. Aggison reports grants from NIH, Michael E. DeBakey Department of Surgery Faculty Research Award, and Roderick D. MacDonald Research Fund during the conduct of the study. No disclosures were reported by the other authors.

Authors' Contributions

Y. Xu: Conceptualization, data curation, formal analysis, investigation, methodology, writing–original draft, writing–review and editing. **C.G. Medina:** Conceptualization, data curation, formal analysis, validation, methodology, writing–original draft, writing–review and editing. **D.R. Surman:** Data curation, formal analysis, investigation, methodology, writing–review and editing. **L.E. Dobrolecki:** Resources, data curation, formal analysis, methodology, writing–review and editing. **M. Vilchis:** Data curation, methodology, writing–review and editing. **M. Ramineni:** Data curation, formal analysis, methodology, writing–review and editing. **S.G. Hilsenbeck:** Data curation, formal analysis, methodology, writing–review and editing. **Y. Li:** Data curation, formal analysis, methodology, writing–review and editing. **N. Li:** Data curation, formal analysis, methodology, writing–review and editing. **S. Wu:** Data curation, formal analysis, methodology, writing–review and editing. **J.C. Aggison:** Data curation, methodology, writing–review and editing. **X. Chen:** Data curation, formal analysis, methodology, writing–review and editing. **Y. Zhu:** Resources, supervision, validation, writing–review and editing. **Y.H. Shen:** Resources, supervision, validation, writing–review and editing. **R.T. Ripley:** Conceptualization, resources, supervision, funding acquisition, project administration, writing–review and editing.

Acknowledgments

This work was supported by the NIH R03 Award (R03 CA252685-01), the NIH R21 Award (R21 CA256466), NIH R37 Award (R37 CA289419), and NIH R01 Award (MPI-R01 CA290173); Michael E. DeBakey Department of Surgery Faculty Research Award; and Roderick D. MacDonald Research Fund at Baylor St. Luke's Medical Center. This project was supported by the Cytometry and Cell Sorting Core at Baylor College of Medicine (BCM) with funding from the Cancer Prevention and Research Institute of Texas (CPRIT) Core Facility Support Award (CPRIT-RP180672), the NIH (CA125123 and RR024574), and the assistance of Joel M. Sederstrom; Pathology and Histology Core at BCM with funding from the Dan L. Duncan Comprehensive Cancer Center NIH grant [P30 Cancer Center Support Grant (NCI-CA125123)]; Patient-Derived Xenograft Core at BCM with funding from P30 Cancer Center Support Grant NCI-CA125123; CPRIT Core Facilities Support Grant RP220646; and Mouse Metabolism and Phenotyping Core at BCM with funding from NIH UM1HG006348, NIH R01DK114356, and NIH R01HL130249. This work was supported by Dan L. Duncan Comprehensive Cancer Center grant (CA P30125123). Continuation and Expansion of National Mesothelioma Virtual Bank for Translational Research (U24-OH009077-15-00 / PI: Dr. Michael Becich / Site PI: R. Taylor Ripley).

Note

Supplementary data for this article are available at Molecular Cancer Therapeutics Online (http://mct.aacrjournals.org/).

Received October 1, 2024; revised February 21, 2025; accepted August 4, 2025; posted first August 13, 2025.

References

1. Vogelzang NJ, Rusthoven JJ, Symanowski J, Denham C, Kaukel E, Ruffie P, et al. Phase III study of pemetrexed in combination with cisplatin versus cisplatin alone in patients with malignant pleural mesothelioma. J Clin Oncol 2023;41:2125–33.
2. Baas P, Scherpereel A, Nowak AK, Fujimoto N, Peters S, Tsao AS, et al. First-line nivolumab plus ipilimumab in unresectable malignant pleural mesothelioma (CheckMate 743): a multicentre, randomised, open-label, phase 3 trial. Lancet 2021;397:375–86.
3. Tait SWG, Green DR. Mitochondria and cell death: outer membrane permeabilization and beyond. Nat Rev Mol Cell Biol 2010;11:621–32.
4. Potter DS, Letai A. To prime, or not to prime: that is the question. Cold Spring Harb Symp Quant Biol 2016;81:131–40.
5. Särchen V, Shanmugalingam S, Kehr S, Reindl LM, Greze V, Wiedemann S, et al. Pediatric multicellular tumor spheroid models illustrate a therapeutic potential by combining BH3 mimetics with Natural Killer (NK) cell-based immunotherapy. Cell Death Discov 2022;8:11.
6. Bhatt S, Pioso MS, Olesinski EA, Yilma B, Ryan JA, Mashaka T, et al. Reduced mitochondrial apoptotic priming drives resistance to BH3 mimetics in acute myeloid leukemia. Cancer Cell 2020;38:872–90.e6.
7. Surman DR, Xu Y, Lee M-J, Trepel J, Brown K, Ramineni M, et al. Therapeutic synergy in esophageal cancer and mesothelioma is predicted by dynamic BH3 profiling. Mol Cancer Ther 2021;20:1469–80.
8. Xu Y, Surman DR, Diggs L, Xi S, Gao S, Gurusamy D, et al. Bile acid-induced "Minority MOMP" promotes esophageal carcinogenesis while maintaining apoptotic resistance via Mcl-1. Oncogene 2020;39:877–90.
9. Mukherjee N, Skees J, Todd KJ, West DA, Lambert KA, Robinson WA, et al. MCL1 inhibitors S63845/MIK665 plus Navitoclax synergistically kill difficult-to-treat melanoma cells. Cell Death Dis 2020;11:443.
10. Abdul Rahman SF, Azlan A, Lo KW, Azzam G, Mohana-Kumaran N. Dual inhibition of anti-apoptotic proteins BCL-XL and MCL-1 enhances cytotoxicity of Nasopharyngeal carcinoma cells. Discov Oncol 2022;13:9.
11. Del Poeta G., Postorino M, Pupo L, Del Principe MI, Dal Bo M, Bittolo T, et al. Venetoclax: Bcl-2 inhibition for the treatment of chronic lymphocytic leukemia. Drugs Today (Barc) 2016;52:249–60.
12. Cleary J.M., Lima CMSR, Hurwitz HI, Montero AJ, Franklin C, Yang J, et al. A phase I clinical trial of navitoclax, a targeted high-affinity Bcl-2 family inhibitor, in combination with gemcitabine in patients with solid tumors. Invest New Drugs 2014;32:937–45.
13. Yuda J., Will C, Phillips DC, Abraham L, Alvey C, Avigdor A, et al. Selective MCL-1 inhibitor ABBV-467 is efficacious in tumor models but is associated with cardiac troponin increases in patients. Commun Med (Lond) 2023;3:154.
14. Ryan J, Montero J, Rocco J, Letai A. iBH3: simple, fixable BH3 profiling to determine apoptotic priming in primary tissue by flow cytometry. Biol Chem 2016;397:671–8.
15. Del Gaizo Moore V, Letai A. BH3 profiling–measuring integrated function of the mitochondrial apoptotic pathway to predict cell fate decisions. Cancer Lett 2013;332:202–5.
16. Ni Chonghaile T, Sarosiek KA, Vo T-T, Ryan JA, Tammareddi A, Moore VDG, et al. Pretreatment mitochondrial priming correlates with clinical response to cytotoxic chemotherapy. Science 2011;334:1129–33.
17. Tron AE, Belmonte MA, Adam A, Aquila BM, Boise LH, Chiarparin E, et al. Discovery of Mcl-1-specific inhibitor AZD5991 and preclinical activity in multiple myeloma and acute myeloid leukemia. Nat Commun 2018;9:5341.
18. Tao Z-F, Hasvold L, Wang L, Wang X, Petros AM, Park CH, et al. Discovery of a potent and selective BCL-XL inhibitor with in vivo activity. ACS Med Chem Lett 2014;5:1088–93.
19. Ryan J, Letai A. BH3 profiling in whole cells by fluorimeter or FACS. Methods 2013;61:156–64.
20. Ianevski A, He L, Aittokallio T, Tang J. SynergyFinder: a web application for analyzing drug combination dose-response matrix data. Bioinformatics 2020;36:2645.
21. Lv X, Dobrolecki LE, Ding Y, Rosen JM, Lewis MT, Chen X. Orthotopic transplantation of breast tumors as preclinical models for breast cancer. J Vis Exp 2020;159:e61173.
22. Husain AN, Colby TV, Ordóñez NG, Allen TC, Attanoos RL, Beasley MB, et al. Guidelines for pathologic diagnosis of malignant mesothelioma 2017 update of the Consensus Statement from the International mesothelioma interest Group. Arch Pathol Lab Med 2018;142:89–108.

23. Potter DS, Du R, Bohl SR, Chow K-H, Ligon KL, Bueno R, et al. Dynamic BH3 profiling identifies pro-apoptotic drug combinations for the treatment of malignant pleural mesothelioma. Nat Commun 2023;14:2897.
24. Olesinski EA, Bhatt S. Dynamic BH3 profiling method for rapid identification of active therapy in BH3 mimetics resistant xenograft mouse models. STAR Protoc 2021;2:100461.
25. Xu D, Liang S-Q, Yang Z, Yang H, Bruggmann R, Oberhaensli S, et al. Malignant pleural mesothelioma co-opts BCL-X(L) and autophagy to escape apoptosis. Cell Death Dis 2021;12:406.
26. Soderquist RS, Crawford L, Liu E, Lu M, Agarwal A, Anderson GR, et al. Systematic mapping of BCL-2 gene dependencies in cancer reveals molecular determinants of BH3 mimetic sensitivity. Nat Commun 2018;9:3513.
27. Campbell KJ, Mason SM, Winder ML, Willemsen RBE, Cloix C, Lawson H, et al. Breast cancer dependence on MCL-1 is due to its canonical anti-apoptotic function. Cell Death Differ 2021;28:2589–600.
28. Potter DS, Du R, Bhola P, Bueno R, Letai A. Dynamic BH3 profiling identifies active BH3 mimetic combinations in non-small cell lung cancer. Cell Death Dis 2021;12:741.
29. Anilkumar U, Khacho M, Cuillerier A, Harris R, Patten DA, Bilen M, et al. MCL-1^{Matrix} maintains neuronal survival by enhancing mitochondrial integrity and bioenergetic capacity under stress conditions. Cell Death Dis 2020;11:321.
30. Perciavalle RM, Stewart DP, Koss B, Lynch J, Milasta S, Bathina M, et al. Anti-apoptotic MCL-1 localizes to the mitochondrial matrix and couples mitochondrial fusion to respiration. Nat Cell Biol 2012;14:575–83.
31. Vander Heiden MG, Chandel NS, Williamson EK, Schumacker PT, Thompson CB. Bcl-xL regulates the membrane potential and volume homeostasis of mitochondria. Cell 1997;91:627–37.
32. Nguyen TTM, Gadet R, Lanfranchi M, Lahaye RA, Yandiev S, Lohez O, et al. Mitochondrial Bcl-xL promotes brain synaptogenesis by controlling non-lethal caspase activation. iScience 2023;26:106674.
33. Durel B, Kervrann C, Bertolin G. Quantitative dSTORM super-resolution microscopy localizes Aurora kinase A/AURKA in the mitochondrial matrix. Biol Cell 2021;113:458–73.
34. Dewitt DA, Hurd JA, Fox N, Townsend BE, Griffioen KJS, Ghribi O, et al. Peri-nuclear clustering of mitochondria is triggered during aluminum maltolate induced apoptosis. J Alzheimers Dis 2006;9:195–205.
35. Mori MP, Penjweini R, Ma J, Alspaugh G, Andreoni A, Kim Y-C, et al. Mitochondrial respiration reduces exposure of the nucleus to oxygen. J Biol Chem 2023;299:103018.
36. Sturm G, Karan KR, Monzel AS, Santhanam B, Taivassalo T, Bris C, et al. OxPhos defects cause hypermetabolism and reduce lifespan in cells and in patients with mitochondrial diseases. Commun Biol 2023;6:22.
37. Tao S, Yang T, Yin Y, Zhang Q. Mitochondrial reactive oxygen species promote mitochondrial damage in high glucose-induced dysfunction and apoptosis of human dental pulp cells. J Dent Sci 2024;19:292–302.
38. Tantawy SI, Sarkar A, Hubner S, Tan Z, Wierda WG, Eldeib A, et al. Mechanisms of MCL-1 protein stability induced by MCL-1 antagonists in B-cell Malignancies. Clin Cancer Res 2023;29:446–57.
39. Montero J, Sarosiek KA, DeAngelo JD, Maertens O, Ryan J, Ercan D, et al. Drug-induced death signaling strategy rapidly predicts cancer response to chemotherapy. Cell 2015;160:977–89.
40. Arulananda S, O'Brien M, Evangelista M, Harris TJ, Steinohrt NS, Jenkins LJ, et al. BCL-XL is an actionable target for treatment of malignant pleural mesothelioma. Cell Death Discov 2020;6:114.
41. Arulananda S, O'Brien M, Evangelista M, Jenkins LJ, Poh AR, Walkiewicz M, et al. A novel BH3-mimetic, AZD0466, targeting BCL-XL and BCL-2 is effective in pre-clinical models of malignant pleural mesothelioma. Cell Death Discov 2021;7:122.
42. Jackson MR, Ashton M, Koessinger AL, Dick C, Verheij M, Chalmers AJ. Mesothelioma cells depend on the antiapoptotic protein Bcl-xL for survival and are sensitized to ionizing radiation by BH3-mimetics. Int J Radiat Oncol Biol Phys 2020;106:867–77.
43. Abdul Rahman SF, Muniandy K, Soo YK, Tiew EYH, Tan KX, Bates TE, et al. Co-inhibition of BCL-XL and MCL-1 with selective BCL-2 family inhibitors enhances cytotoxicity of cervical cancer cell lines. Biochem Biophys Rep 2020;22:100756.
44. Heimer S, Knoll G, Neubert P, Hammer KP, Wagner S, Bauer RJ, et al. Hypertonicity counteracts MCL-1 and renders BCL-XL a synthetic lethal target in head and neck cancer. FEBS J 2021;288:1822–38.
45. Varin E., Denoyelle C, Brotin E, Meryet-Figuière M, Giffard F, Abeilard E, et al. Downregulation of Bcl-xL and Mcl-1 is sufficient to induce cell death in mesothelioma cells highly refractory to conventional chemotherapy. Carcinogenesis 2010;31:984–93.
46. Moyzis AG, Lally NS, Liang W, Leon LJ, Najor RH, Orogo AM, et al. Mcl-1-mediated mitochondrial fission protects against stress but impairs cardiac adaptation to exercise. J Mol Cell Cardiol 2020;146:109–20.
47. Widden H, Placzek WJ. The multiple mechanisms of MCL1 in the regulation of cell fate. Commun Biol 2021;4:1029.
48. Tornero D, Posadas I., Ceña V. Bcl-x(L) blocks a mitochondrial inner membrane channel and prevents Ca2+ overload-mediated cell death. PLoS One 2011;6:e20423.
49. Morciano G, Giorgi C, Balestra D, Marchi S, Perrone D, Pinotti M, et al. Mcl-1 involvement in mitochondrial dynamics is associated with apoptotic cell death. Mol Biol Cell 2016;27:20–34.
50. Lacombe A, Scorrano L. The interplay between mitochondrial dynamics and autophagy: from a key homeostatic mechanism to a driver of pathology. Semin Cell Dev Biol 2024;161-162:1–19.
51. Huang C-R, Yang-Yen H-F. The fast-mobility isoform of mouse Mcl-1 is a mitochondrial matrix-localized protein with attenuated anti-apoptotic activity. FEBS Lett 2010;584:3323–30.
52. Tantawy SI, Timofeeva N, Sarkar A, Gandhi V. Targeting MCL-1 protein to treat cancer: opportunities and challenges. Front Oncol 2023;13:1226289.